BIOCHEMISTRY

 Volume 45, Number 40 October 10, 2006

Articles

Catalytic Mechanism of *S*-Ribosylhomocysteinase: Ionization State of Active-Site Residues†

Jinge Zhu,‡ Sushilla Knottenbelt,§ Martin L. Kirk,§ and Dehua Pei*,‡

Department of Chemistry and Ohio State Biochemistry Program, The Ohio State University, 100 West 18th Avenue, Columbus, Ohio 43210, and Department of Chemistry, University of New Mexico, Albuquerque, New Mexico 87131

Received July 15, 2006; Revised Manuscript Received August 21, 2006

ABSTRACT: *S*-Ribosylhomocysteinase (LuxS) catalyzes the cleavage of the thioether linkage in *S*-ribosylhomocysteine (SRH) to produce homocysteine (Hcys) and 4,5-dihydroxy-2,3-pentanedione (DPD), the precursor of type II bacterial autoinducer (AI-2). The proposed catalytic mechanism involves two consecutive ribose carbonyl migration steps via an intramolecular redox reaction and a subsequent β-elimination step, all catalyzed by a divalent metal ion (e.g., Fe^{2+} or Co^{2+}) and two general acids/bases in the active site. Absorption and EPR spectroscopic studies were performed with both wild-type and various mutant forms of LuxS under a wide range of pH conditions. The studies revealed a pK_a of 10.4 for the metal-bound water. The pK_a value of Cys-83 was determined to be <6 by $^{13}C-^{1}H$ HSQC NMR experiments with [3-^{13}C]cysteine-labeled Zn^{2+}-substituted *Escherichia coli* LuxS. The active form of LuxS contains a metal-bound water and a thiolate ion at Cys-83, consistent with the proposed roles of the metal ion (Lewis acid) and Cys-83 (general acid/base) during catalysis. Finally, an invariant Arg-39 in the active site was demonstrated to be at least partially responsible for stabilizing the thiolate anion of Cys-83.

S-Ribosylhomocysteinase (LuxS) is a key enzyme involved in the biosynthesis of type II autoinducer (AI-2),[1] which is thought to act as a universal signal for interspecies communication among both Gram-positive and Gram-negative bacteria (*1*, *2*). AI-2 biosynthesis starts from *S*-adenosylhomocysteine (SAH), a byproduct of numerous *S*-adenosylmethionine (SAM)-dependent methyltransferase reactions. Hydrolysis of SAH by nucleosidase Pfs yields adenine and *S*-ribosylhomocysteine (SRH) (Figure 1). Subsequently, SRH is cleaved by LuxS to produce homocysteine (Hcys) and 4,5-dihydroxy-2,3-pentanedione (DPD) (*3*−*5*). DPD undergoes spontaneous cyclization and rearrangement into several furanone forms (*5*). For *Salmonella typhimurium*, the active AI-2 form is (2*R*,4*S*)-2-methyl-2,3,3,4-tetrahydroxytetrahydrofuran (*6*), whereas *Vibrio harveyi* utilizes a borate diester of (2*S*,4*S*)-2-methyl-2,3,3,4-tetrahydroxytetrahydrofuran as its active AI-2 (*7*). The active AI-2 form(s) detected by other bacteria remains to be determined.

The high-resolution X-ray crystal structures of LuxS from *Helicobacter pylori*, *Deinococcus radiodurans*, *Haemophilus influenzae*, and *Bacillus subtilis* revealed that LuxS exists

† This work was supported by grants from the National Institutes of Health (AI62901 to D.P. and GM-057378 to M.L.K.).

* To whom correspondence should be addressed: Department of Chemistry, The Ohio State University, 100 W. 18th Ave., Columbus, OH 43210. Phone: (614) 688-4068. Fax: (614) 292-1532. E-mail: pei.3@osu.edu.

‡ The Ohio State University.

§ University of New Mexico.

[1] Abbreviations: AI, autoinducer; SAH, *S*-adenosylhomocysteine; SAM, *S*-adenosylmethionine; SRH, *S*-ribosylhomocysteine; Hcys, homocysteine; DPD, 4,5-dihydroxy-2,3-pentanedione; DTNB, 5,5′-dithiobis(2-nitrobenzoic acid); BsLuxS, *B. subtilis* LuxS; EcLuxS, *E. coli* LuxS; VhLuxS, *V. harveyi* LuxS; GA/GB, general acid/general base; EPR, electron paramagnetic resonance; HSQC, heteronuclear single-quantum correlation.

10.1021/bi061434v CCC: $33.50
Published on Web 09/16/2006

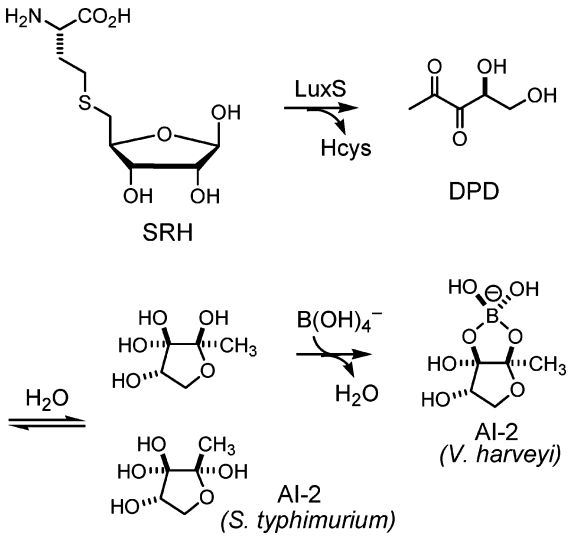

FIGURE 1: Function of LuxS in the biosynthetic pathway of AI-2.

as a homodimer with two identical active sites at the dimer interface (*8*−*12*). Each active site contains a tetrahedrally coordinated divalent metal ion, which has been demonstrated to be Fe^{2+} in *B. subtilis* LuxS (BsLuxS) (*13*). The metal ion is coordinated with three conserved residues (His-54, His-58, and Cys-126 in BsLuxS) and a hydroxide/water molecule. Substitution of Co^{2+} preserves full catalytic activity, whereas the Zn^{2+}-substituted form has ∼10% of the activity of the native enzyme (*13*). The proposed catalytic mechanism involves two consecutive carbonyl migration reactions followed by a β-elimination reaction (Figure 2) (*11*−*15*). Since free SRH exists predominantly in its hemiacetal form, it was proposed that binding to the LuxS active site would open the ribose ring so that the carbonyl oxygen of the aldehyde binds to the metal ion, displacing a bound water/hydroxide molecule in the free enzyme. Abstraction of a proton from the C2 position by a general base (likely Cys-84 in BsLuxS) generates a *cis*-enediolate intermediate (**2**). Ligand exchange from the C1 to C2 OH group, presumably assisted by a second base/acid (likely Glu-57) via a five-membered ring transition state, gives enediolate **3**. Reprotonation at C1 by Cys-84 and enol−keto tautomerism generate a 2-keto intermediate (**4**). Repetition of the sequence described above results in the migration of the carbonyl group to the C3 position to give a 3-keto intermediate (**7**). Subsequent β-elimination, probably catalyzed by Glu-57 (or a third acid/base), releases Hcys and the enol form of DPD (**9**). Enol **9** spontaneously tautomerizes to the keto form, either on its way to or after leaving the active site.

This mechanism is supported by substantial experimental evidence, including the demonstrated intermediacy of ketones **4** and **7** (*14*), direct coordination of the 2-keto oxygen of intermediate **4** to the metal ion (*11*), and confirmation of the proposed stereochemical course of the proton transfer reactions (*15*). However, some important issues remain to be resolved. First, the proposed mechanism begins with the displacement of a metal-bound H_2O/OH^- by the aldehyde carbonyl group of SRH. Since a hydroxide ion is expected to bind to the metal ion much more tightly than a water molecule, we theorized that the pK_a of the M−H_2O species should be sufficiently high that the M−H_2O species dominates at physiological pH. Second, since the first chemical step involves abstraction of a proton from C2 by Cys-84, the pK_a value of Cys-84 should be less than 7. This in turn raises the question of what stabilizes the thiolate ion in the enzyme active site. In this work, we determined the pK_a value of the metal-bound water to be ∼10 by monitoring the

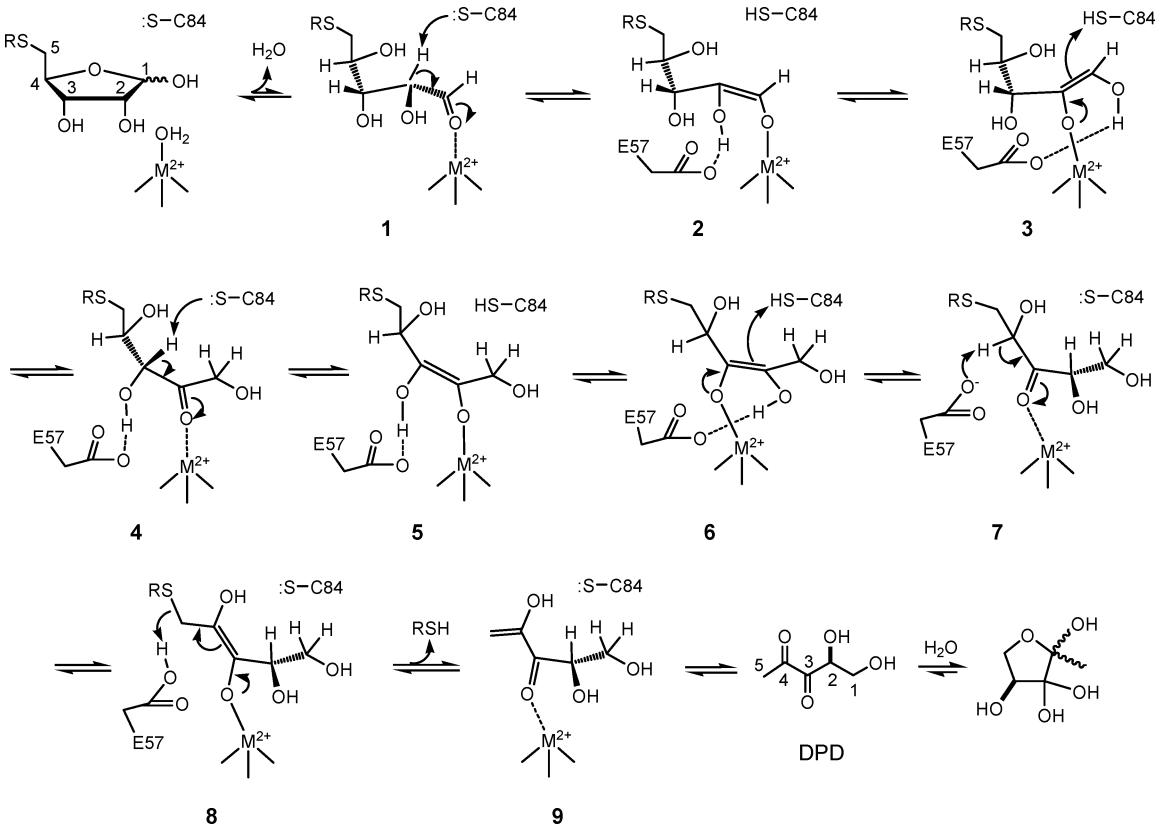

FIGURE 2: Proposed catalytic mechanism of the LuxS reaction. RSH is Hcys.

absorption spectra of Co^{2+}-substituted LuxS as a function of pH. A pK_a of <6 was also determined for Cys-83 (equivalent to Cys-84 in BsLuxS) of *Escherichia coli* LuxS (EcLuxS) by $^{13}C-^{1}H$ heteronuclear single-quantum correlation (HSQC) NMR spectroscopy of [3-^{13}C]Cys-labeled EcLuxS. The function of several other active-site residues has also been examined by site-directed mutagenesis and by monitoring the absorption and EPR spectra of the mutants as a function of pH. Arg-39 was found to be at least partially responsible for the low pK_a of Cys-83.

MATERIALS AND METHODS

Materials. Wild-type and mutant Co^{2+}- and Zn^{2+}-substituted LuxS variants from *B. subtilis*, *E. coli*, and *V. harveyi* were overexpressed in *E. coli* and purified to near homogeneity as described previously (*11*, *13*−*16*). Oligonucleotides were purchased from Integrated DNA Technologies (Coralville, IA) and Invitrogen (Carlsbad, CA). L-Cysteine (3-^{13}C, 99%) and D_2O (99.9%) were purchased from Cambridge Isotope Laboratories (Andover, MA). The 2-ketone intermediate (**4**) was synthesized as previously described (*14*). All other chemicals and reagents were purchased from Sigma-Aldrich (St. Louis, MO).

LuxS Mutants. The gene encoding EcLuxS was subcloned from the plasmid pET22b-EcLuxS−HT (*16*) using primers 5′-GGAAGGCCATATGCCGTTGTTAGATAGCTTC-3′ and 5′-GGGAATTCATAGTTTACTGACTAGATGTGCAGTTCC-3′. The PCR product was digested with restriction endonucleases *Nde*I and *Eco*RI and cloned into the pET22b(+) vector (Novagen, Madison, WI) to generate the non-His-tagged EcLuxS construct, pET22b-EcluxS. Site-directed mutagenesis was carried out on plasmids pET22b-BsluxS-HT for BsLuxS (*13*), pET22b-VhluxS-HT for *V. harveyi* LuxS (VhLuxS) (*14*), and pET22b-EcluxS (non-His-tagged) for EcLuxS using the QuikChange mutagenesis kit (Stratagene, La Jolla, CA). The following mutagenesis primers were used: BsLuxS-S6A, 5′-CATATGCCTTCAGTAGAAGCTTTTGAGCTTGATCATAATG-3′; BsLuxS-H11Q, 5′-GAAAGTTTTGAGCTTGATCAAAATGCGGTTGTTGCTC-3′; BsLuxS-R39M, 5′-GATAATAAATTTGATATTATGTTTTGCCAGCCAAATAAAC-3′; BsLuxS-Y89F, 5′-TGCCAAACAGGCTATTTTCTTGTTGTGAGCGGA-3′; EcLuxS-C41A, 5′-GTTCGATCTGCGCTTCGCCGTGCCGAACAAAGAAG-3′; and EcLuxS-C83D, 5′-GATATCTCGCCAATGGGCGACCGCACCGGTTTTTATATG-3′. The identity of all DNA constructs was confirmed by DNA sequencing. Other LuxS mutants used in this work were reported previously (*11*, *13*, *14*).

LuxS Activity Assay. The LuxS reaction was performed in a buffer containing 50 mM HEPES (pH 7.0), 150 mM NaCl, 150 μM 5,5′-dithiobis(2-nitrobenzoic acid) (DTNB) (*17*), and varying concentrations of SRH (0−200 μM) or 2-ketone **4** (0−130 μM). The reaction (total volume of 1 mL) was initiated by the addition of Co^{2+}-substituted VhLuxS (Co−VhLuxS, final concentration of 0.5 μM) and monitored continuously at 412 nm (ϵ = 14 150 M^{-1} cm^{-1}) in a Perkin-Elmer λ25 UV−vis spectrophotometer at room temperature. The initial rates calculated from the early regions of the progress curves (usually 30 s) were fitted against the Michaelis−Menten equation $V = k_{cat}[E]_0[S]/(K_M + [S])$ using KaleidaGraph 3.5 to obtain the k_{cat} and K_M values. When the LuxS activity of certain mutants was too low for k_{cat} and K_M values to be determined separately, data were fitted against the Lineweaver−Burk equation $1/V = K_M/(k_{cat}[E]_0) \times 1/[S] + 1/(k_{cat}[E]_0)$ to estimate k_{cat}/K_M values. For some mutants, the reaction product DPD was converted into its quinoxaline derivative and isolated as described previously (*13*−*15*). Briefly, 1 mM SRH, 5 mg/mL Co−LuxS variant, and 1 mM 1,2-phenylenediamine were mixed in a pH 7 buffer and incubated for 24 h. An additional 1 equiv of 1,2-phenylenediamine was then added, and the resulting solution was incubated at pH 4−5 for an additional 24 h followed by ethyl acetate extraction.

UV−Vis Spectroscopy. Co−LuxS variants were dialyzed against a Cl^--free buffer [75 mM HEPES (pH 7.8)] at 4 °C overnight with three changes of the buffer. After brief centrifugation to remove any precipitate if necessary, the protein solution was diluted into buffers with various pH values to produce a final concentration of 60−80 μM. The following buffers were used: 50 mM MES for pH 6.5, 50 mM Bis-Tris for pH 6.5−7.0, 50 mM HEPES for pH 7.0−8.0, 50 mM CHES for pH 8.5−9.5, and 50 mM CAPS for pH 10.0−12.0. The buffers were adjusted to the appropriate pH values with NaOH or acetic acid. Absorption spectra (800−300 nm) were recorded on a Perkin-Elmer λ25 UV−vis spectrophotometer at room temperature. Molar absorptivity (ϵ_{obs}) at a specific wavelength was plotted against pH and fitted against the Henderson−Hasselbalch equation $\epsilon_{obs} = \epsilon_A + (\epsilon_{HA} - \epsilon_A) \times 10^{-pH}/(10^{-pH} + 10^{-pK_a})$ (*18*) using KaleidaGraph 3.6 to give the pK_a values for each LuxS variant, where ϵ_{HA} and ϵ_A are the molar absorptivities of the fully protonated and deprotonated forms, respectively.

EPR Spectroscopy. Frozen glass EPR spectra were measured on a Bruker model EMX spectrometer operating at X-band (~9.3 GHz). A microwave power of 0.2 mW was used for all experiments, and spectra were collected at 8 K using an Oxford Instruments liquid helium flow cryostat. Final enzyme concentrations of ~3 mg/mL were used with 20% (w/v) PEG8000 as a cryoprotectant. The enzyme solutions used in the EPR studies were kept either at pH 8 in 80 mM HEPES buffer or at pH 11 in 500 mM CAPS buffer. Addition of the cryoprotectant did not degrade the protein.

Preparation of [3-^{13}C]Cys-Labeled Zn^{2+}-Substituted EcLuxS (Non-His-Tagged). *E. coli* BL21(DE3) cells carrying the appropriate plasmid DNAs were grown in minimal medium supplemented with 75 mg/L ampicillin, 0.25% D-glucose, 2 μg/mL thiamin, 1 μg/mL D-biotin, 0.1% $(NH_4)_2SO_4$, and a metal salt mixture [0.5 mM $MgSO_4$, 0.5 μM $CaCl_2$, 0.1 μM $MnCl_2$, 0.5 μM H_3BO_3, 10 nM $CuSO_4$, and 1 nM $(NH_4)_6Mo_7O_{24}$] at 37 °C to an OD_{600} of 0.9. The cells were induced by the addition of 200 μM isopropyl β-D-thiogalactoside and continued to grow at 30 °C for an additional 4 h. At the time of induction, 100 μM $ZnCl_2$, 30−40 mg/L [3-^{13}C]Cys, 0.41 mg/L Leu, and Ala, Ile, and Val (1.66 mg/L each) were added to the growth medium to produce [3-^{13}C]Cys-labeled Zn^{2+}-substituted LuxS. Supplementation of Ala, Ile, Leu, and Val helped suppress the scrambling of the [3-^{13}C]Cys label (*19*). Cells were harvested by centrifugation and resuspended in the lysis buffer (25 mL/L of culture) containing 25 mM Tris (pH 7.6), 20 mM NaCl, 1% Triton X-100, 0.5% protamine sulfate, 40 μg/mL trypsin inhibitor, and 150 μg/mL chicken egg white lysozyme. The cells were lysed by

Table 1: Catalytic Properties of Co−LuxS Variants toward SRH and 2-Ketone **4**[a]

	SRH				2-ketone **4**			
	k_{cat} (s^{-1})	K_M (μM)	k_{cat}/K_M (M^{-1} s^{-1})	relative activity (%)	k_{cat} (s^{-1})	K_M (μM)	k_{cat}/K_M ($M^{-1}s^{-1}$)	relative activity (%)
WT[b]	0.40 ± 0.01	39 ± 1	1.0×10^4	100	0.40 ± 0.02	38 ± 1	1.0×10^4	100
WT (Ec)	0.40 ± 0.02	16 ± 2	2.5×10^4	100	ND[d]	ND[d]	ND[d]	ND[d]
S6A[c]	0.031 ± 0.001	45 ± 2	6.9×10^2	6.9	0.102 ± 0.002	96 ± 7	1.1×10^3	11
H11Q[c]	ND[d]	ND[d]	10	0.1	0.008 ± 0.001	39 ± 2	2.0×10^2	2.0
R39M[c]	ND[d]	ND[d]	8	0.08	0.008 ± 0.001	22 ± 2	3.5×10^2	3.5
C41A (Ec)	0.38 ± 0.04	16 ± 3	2.4×10^4	96	ND[d]	ND[d]	ND[d]	ND[d]
C83D[b]	ND[d]	ND[d]	4	0.04	0.005 ± 0.001	50 ± 4	1.1×10^2	1.1
C83S[b]	ND[d]	ND[d]	14	0.14	0.024 ± 0.001	58 ± 3	4.1×10^2	4.1
R39M/C83D	ND[d]	ND[d]	3	0.03	0.005 ± 0.001	17 ± 1	2.7×10^2	2.7
R39M/C83S	ND[d]	ND[d]	2	0.02	0.004 ± 0.001	63 ± 4	6.6 × 10	0.66

[a] Unless otherwise indicated, activities reported were for Co−VhLuxS. [b] Data from ref *14*. [c] Data from ref *11*. [d] Not determined.

being stirred for 20 min at 4 °C, followed by brief sonication and centrifugation. The supernatant was loaded on a Q-Sepharose Fast-Flow column (2.5 cm × 13 cm; Amersham Pharmacia Biotech AB) pre-equilibrated in 25 mM Tris (pH 7.6) and 20 mM NaCl. The column was washed with 200 mL of the equilibrating buffer and eluted with a NaCl gradient (from 20 to 500 mM) in the buffer described above. Fractions containing a significant amount of LuxS protein (as analyzed by 12% SDS−PAGE) were pooled, concentrated in an Amicon ultrafiltration cell or ultracentrifugal filter device (Millipore), quickly frozen in a 2-propanol/dry ice bath, and stored at −80 °C. Protein concentrations were determined by the Bradford method (*20*) using bovine serum albumin as a standard and corrected by a factor of 0.5 (*16*). Protein yields were typically 80−100 mg/L of culture.

$^{13}C-^{1}H$ HSQC Spectroscopy. [3-^{13}C]Cys-labeled Zn^{2+}-substituted EcLuxS (non-His-tagged) was diluted in 100 mM sodium phosphate buffers at various pH values to give a final concentration of ~1 mM. D_2O (60−100 μL) was added to the sample to yield a 10−15% D_2O fraction in a total volume of 500−600 μL. Final pH values were confirmed with accurate pH paper (EMD) on the authentic solutions and with a pH meter on blank buffers without protein. $^{13}C-^{1}H$ HSQC spectra were collected on a Bruker DMX 600 MHz instrument over the pH range of 6.0−9.5 at 37 °C under identical settings for each sample. The ^{13}C chemical shift was fitted against the Henderson−Hasselbalch equation $\delta_{obs} = \delta_A + (\delta_{HA} - \delta_A) \times 10^{-pH}/(10^{-pH} + 10^{-pK_a})$ (*18*) using KaleidaGraph 3.6 to obtain pK_a values, where δ_{obs} represents the experimentally observed chemical shift values and δ_{HA} and δ_A are the chemical shift values for the fully protonated and deprotonated forms, respectively.

RESULTS

Catalytic Activity of LuxS Mutants. On the basis of sequence alignment and X-ray crystal structures, a series of conserved active-site residues were targeted for mutagenesis in an attempt to assess their roles in substrate binding and catalysis. Mutants were constructed in BsLuxS, VhLuxS, and EcLuxS and produced in both Zn^{2+}- and Co^{2+}-substituted forms for various applications. VhLuxS and EcLuxS are 77% identical in sequence, while the sequence of BsLuxS is 38% identical with both of them. All three proteins exist as homodimers of 37.5 kDa. VhLuxS had the largest k_{cat} and K_M values among the three enzymes (*14*), making it convenient for kinetic characterization. On the other hand, Co−BsLuxS had well-defined absorption spectra in the visible region while Zn−EcLuxS was best behaved for the determination of the Cys-83 pK_a by HSQC NMR spectroscopy (vide infra). The mutants employed in this work include S6A, H11Q, R39M, C41A, E57Q, C84A, C84D, C84S (C83A, C83D, and C83S in VhLuxS and EcLuxS), and Y89F (Table 1). The catalytic activity of these mutants was examined by two different assays. The release of homocysteine was first monitored by the DTNB assay (*16*). For less active mutants, their catalytic activities were confirmed by carrying out the LuxS reaction in the presence of 1,2-phenylenediamine (*13*−*15*). This procedure converted the released DPD into a quinoxaline derivative, which was analyzed by HPLC. Although not quantitative, the latter assay is highly sensitive. With the exception of the C84A mutant, all mutants still possess various levels of catalytic activity toward SRH (0.02−96% of that of the wild type) and the 2-ketone intermediate (**4**) (0.66−11% of that of the wild type) (Table 1). Two double mutants, C83D/R39M and C83S/R39M, were also generated, and their activities were compared to those of the corresponding single mutants. Interestingly, introduction of the R39M mutation into the wild-type enzyme dramatically reduced the catalytic activity (1250-fold toward SRH). This mutation also further reduced the activity of the C83S mutant (7-fold). However, the C83D/R39M mutant had activity similar to that of the C83D enzyme, indicating that mutation of Arg-39 had no further effect on the C83D mutant. This is consistent with a role of Arg-39 in stabilizing the thiolate ion of Cys-83 (and the alkoxide ion of Ser-83). The presence of significant catalytic activity suggests that there are no drastic global structural changes in these mutants. C84A is the only mutant that had no detectable catalytic activity; however, its X-ray crystal structure showed little difference from that of the wild-type enzyme (*11*).

UV−Vis Spectroscopy. The absorption spectrum of Co−BsLuxS was perturbed by many molecules and/or ions, which presumably bound to the active site of LuxS. Therefore, the LuxS proteins were exhaustively dialyzed against a chloride-free buffer to remove any small anions (e.g., Cl^-) that could interfere with their spectra. The buffer materials used in this study were carefully chosen because they do not affect the absorption spectra of LuxS.

The absorption spectra of wild-type Co−BsLuxS were essentially identical at pH 6.5−10. Three absorption bands,

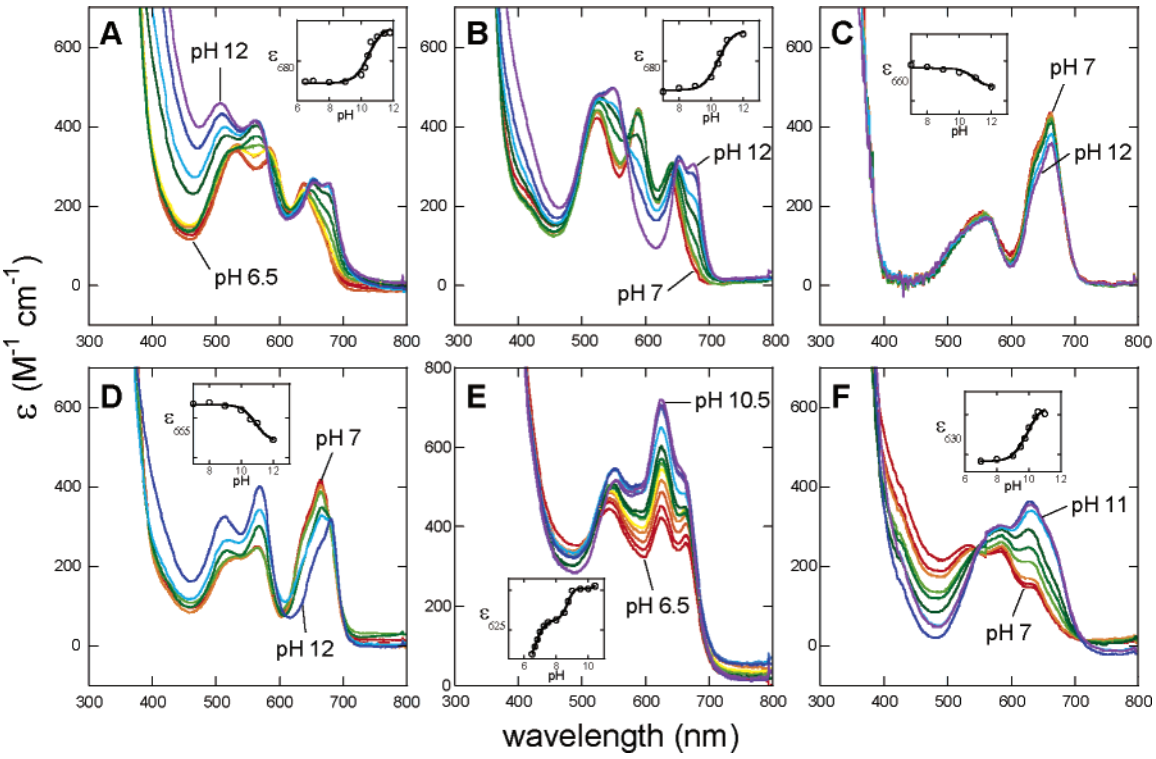

FIGURE 3: Overlaid UV−vis spectra of wild-type and mutant Co−BsLuxS under various pH conditions (pH 6.5−12): (A) wild-type LuxS, (B) C84D LuxS, (C) C84A LuxS, (D) C84S LuxS, (E) R39M LuxS, and (F) R39M/C84D LuxS. Insets are plots of molar absorptivity at the indicated wavelengths vs pH. The curves were fitted to the data as described in Materials and Methods.

derived from the $^4A \rightarrow {}^4T$ ligand field transition, were observed in the visible region of the spectrum at 640, 585, and 530 nm, with extinction coefficients consistent with a tetrahedral active-site geometry ($\epsilon > 300$ M^{-1} cm^{-1}) as observed in X-ray crystal structures (Figure 3A) (*21*). At pH >10, however, the spectra exhibited pH-dependent changes (Figure 3A). First, a shoulder peak appeared at 675 nm as the pH increased and became a well-defined peak at pH 11−12. Second, the peaks at 640 nm red shifted to 650 nm, while two peaks at 530 and 585 nm blue shifted to 510 and 560 nm, respectively. The slight perturbation of the spectra was due to protein denaturation at extreme pH values; it became less stable at pH ≥11 and easily precipitated at pH <7. Very similar spectral changes were observed for wild-type Co−EcLuxS (data not shown). The presence of two isobestic points at 580 and 645 nm indicates a single ionization event with direct interconversion between two species as a function of pH. A plot of the absorbance at 680 nm against pH generated a titration curve with an apparent pK_a value of 10.4 for BsLuxS (Figure 3A, inset) and 10.2 for EcLuxS (data not shown). We tentatively assigned these pK_a values to the metal-bound H_2O ligand. Thus, at pH <10, the spectra represent LuxS with H_2O bound to the metal, whereas at pH 12, the spectra represent the enzyme with metal-bound OH^- in the active site.

As revealed by the X-ray crystal structures of LuxS (*8*−*11*), there are several other potentially ionizable residues in the active site, including Ser-6, His-11, Arg-39, Glu-57, Cys-84, and Tyr-89. To ascertain that the pK_a value of ∼10 in wild-type LuxS is due to the metal-bound H_2O instead of other functional groups in the active site and to evaluate the possible effect of nearby amino acid residues on the pK_a value, the experiments were repeated with LuxS variants containing specific mutations of the residues mentioned above. S6A, H11Q, E57Q, and Y89F LuxS all exhibited sigmoidal titration curves with pK_a values of ∼10 (data not shown). However, mutation of other residues, e.g., Cys-84 and Arg-39, generated distinctive spectral features and a different pH effect.

The absorption spectra of C84D LuxS displayed an overall shape similar to those of the wild-type enzyme and a simple pH titration curve with a pK_a value of 10.4 (Figure 3B). Once again, the spectra at low and high pH represent LuxS with metal-bound H_2O and OH^-, respectively. However, the UV−vis spectra of C84A LuxS were dramatically different from those of wild-type LuxS (Figure 3C). First, the three d−d transition bands appeared at 555, 630, and 660 nm, and the peak at 660 nm became the strongest absorption band. Second, the spectra did not undergo significant pH-dependent changes over the entire pH range of 7−12. Similar absorption spectra were observed for C84S LuxS at pH 7−10 as well, which lacked pH-dependent changes and exhibited strong absorption at 665 nm with a shoulder peak at 630 nm (Figure 3D). As the pH was increased from 10 to 12, however, the strong absorption at 600−700 nm started to decrease and the spectra became very much like those of wild-type LuxS at high pH (Figure 3A,D). Interestingly, the R39M mutant exhibited two ionization events with pK_a values of 8.6 and 6.4 and essentially no change beyond pH 10 (Figure 3E). Finally, the absorption spectra of three LuxS double mutants, R39M/C84D, R39M/C84S, and R39M/C84A, were titrated under the same conditions over the pH range of 7−11. R39M/C84D exhibited pH-dependent spectral changes with a pK_a of 9.9 for the metal-bound water, similar to that observed in the C84D single mutant (Figure 3F), while the spectra of R39M/C84S and R39M/C84A remained essentially unchanged over the entire pH range (data not shown). Together, the UV−vis absorption studies suggest that the

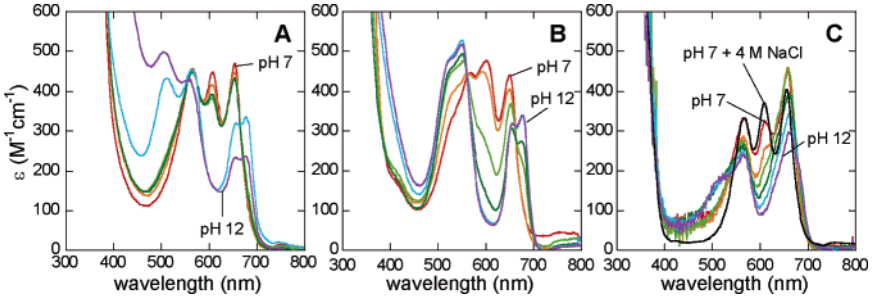

FIGURE 4: Overlaid UV−vis spectra of Co−BsLuxS under various pH conditions (pH 7, 8, 9, 10, 11, or 12) and in the presence of 2 M NaCl: (A) wild-type LuxS, (B) C84D LuxS, and (C) C84A LuxS.

pK_a of metal-bound water is ~10 in wild-type LuxS and the metal-bound water remains in its aqua form at physiological pH, but the value is affected by the nature of certain active-site residues, i.e., amino acids at positions 84 and 39.

Binding of Chloride to Co−LuxS. We found that the Cl^- ion could displace the metal-bound H_2O/OH^- in wild-type LuxS to produce a characteristic Co−Cl spectrum with three absorption bands at 655, 610, and 565 nm of almost equal intensity (Figure 4A). This provides a simple method for comparing the relative affinity of the metal ion for H_2O/OH^- in wild-type and mutant LuxS. Thus, UV−vis spectra were recorded over the pH range of 7−12 in the presence of 2 M NaCl. At pH ≤10, wild-type LuxS existed predominantly in the Co−Cl form; as the pH increased to 11, the Co−OH form dominated (Figure 4A). The pH-titration behavior of C84D LuxS was very similar to that of wild-type LuxS, except that the Co−Cl to Co−OH transition occurred at a slightly lower pH (pH ~9) (Figure 4B). The C84A mutant behaved differently. At pH ≥9, the enzyme existed almost exclusively in the Co−OH form. Even at pH 7.0, the protein was not completely converted into the Co−Cl form (compare with the spectrum at pH 7.0 and with 4 M NaCl) (Figure 4C). The C84S mutant behaved like the C84A protein (data not shown). In a control experiment, addition of 1 M $(NH_4)_2SO_4$ in place of NaCl did not cause a change in any of the spectra (data not shown), indicating that the observed spectral changes were not due to simple alterations of the ionic strength of the solutions. In addition, it was observed that LuxS activity was inhibited by Cl^- at high concentrations, but not by SO_4^{2-} at the same concentrations (up to 1 M). These results are consistent with the hypothesis that wild-type and C84D LuxS exist in the Co−H_2O form at pH <10 whereas the C84A and C84S variants are in the Co−OH form at physiological pH (in the absence of Cl^- ion).

EPR Spectroscopy. EPR spectroscopy is a sensitive probe of ground- and excited-state electronic structure and therefore may be used in conjunction with UV−vis spectroscopy to probe pH and mutation-induced changes at the active site of LuxS. The EPR spectrum of the C84D mutant at pH 8 displayed a characteristic quartet resonance with an only slight deviation from axial symmetry, with a g_1 of 4.8, a g_2 of 4.2, and a g_3 of ~2.12 (Figure 5). Hyperfine coupling to the $I = {}^7/_2$ ^{59}Co nucleus was only resolved on g_3 (A_3^{Co} = 158 MHz). Spectral simulation of the major contributor to the spectrum showed the presence of a slight degree of active-site inhomogeneity, which is presumably responsible for the low-field shoulder on g_1 and the sharp $g = 2$ resonance. EPR magnetic circular dichroism (MCD) and

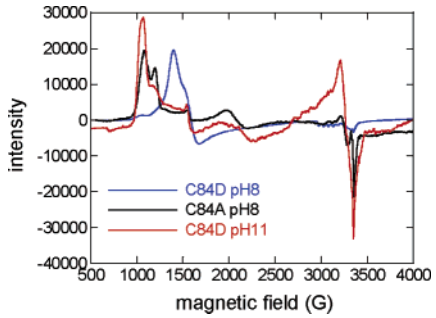

FIGURE 5: EPR spectra of C84D BsLuxS at pH 8 (blue) and 11 (red) and C84A LuxS at pH 8 (black).

variable-temperature, variable-field MCD clearly indicate a high-spin $S = {}^3/_2$ Co(II) ground state consistent with the pseudotetrahedral coordination geometry (S. Knottenbelt and M. L. Kirk, unpublished results).

The EPR spectrum of the C84A mutant at pH 8 was markedly different from that of the C84D mutant at the same pH, and the data indicated greater active-site heterogeneity with at least three components contributing to the overall spectrum. The dominant contribution to the spectrum was considerably more rhombic than that of the C84D mutant. Spectral simulation of this component yielded g_1-g_3 values of 6.20, 3.20, and 2.0, respectively, and no resolvable Co hyperfine splitting on any component of the g-tensor. Exchange into D_2O resulted in no appreciable changes to the spectrum, indicating that the splitting observed at $g \sim 6$ was not due to coupling to an exchangeable proton (i.e., OH^-/H_2O). When the pH is increased to 11, the pseudoaxial C84D mutant spectrum closely resembled that of the C84A mutant at pH 8. Notably, this was manifest by the appearance of an active-site inhomogeneity with one spectral component possessing a rhombic g-tensor with a g_1 of 6.2, a g_2 of 3.20, and a g_3 of 2.0, in remarkable agreement with the dominant species observed in the C84A spectrum collected at pH 8.

The rhombic EPR spectra observed for the C84D and C84A LuxS mutants are consistent with a distorted tetrahedral Co(II) active site (*22*) and are similar to EPR spectra observed for AAP, the aminopeptidase from *Aeromonas proteolytica* (*23*). As suggested for AAP, where g_1-g_3 = 6.82, 2.95, and 1.96, respectively (compare C84A at pH 8; g_1-g_3 = 6.20, 3.20, and 2.00, respectively), the dominant transitions occur primarily within the $m_s = \pm{}^1/_2$ Kramer's doublet of the $S_{total} = {}^3/_2$ Co(II) rhombic spin system. The spectra observed for C84D at pH 8 and C84A at pH 11 are markedly less rhombic but still consistent with an axially distorted $S_{total} = {}^3/_2$ Co(II) site.

$^{13}C-^1H$ HSQC Spectroscopy. To test the role of Cys-83 (EcLuxS) as a general base, $^{13}C-^1H$ HSQC experiments were

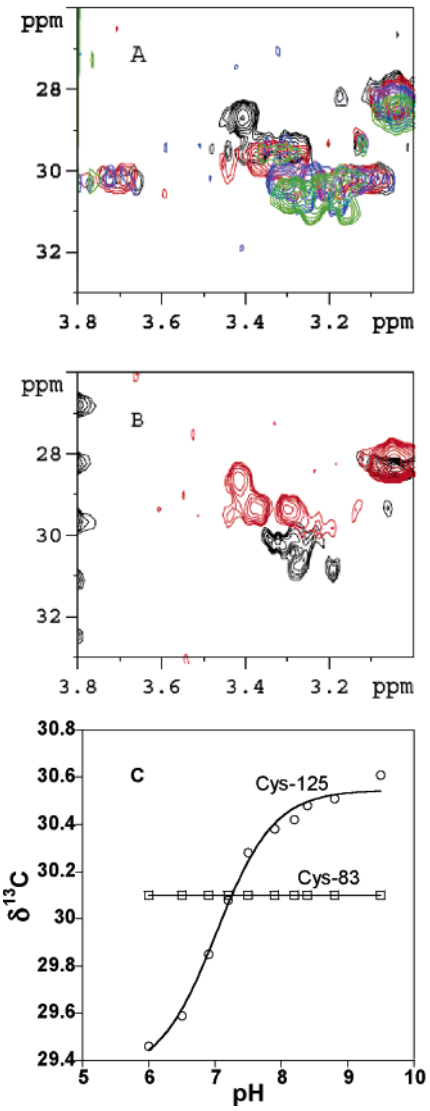

FIGURE 6: pH titration of [3-^{13}C]cysteine-labeled Zn-EcLuxS by ^{13}C−^{1}H HSQC NMR: (A) overlaid NMR spectra of C41A LuxS at pH 8.2 (green), 7.4 (blue), 6.9 (red), and 6.0 (black), (B) overlaid NMR spectra of C41A/C83D LuxS at pH 8.0 (black) and 6.0 (red), and (C) plot of ^{13}C chemical shifts of Cys-83 and Cys-125 in C41A LuxS vs pH.

carried out at varying pH values with [3-^{13}C]Cys-labeled EcLuxS. EcLuxS was chosen for its greater stability and produced good-quality ^{13}C−^{1}H HSQC spectra, which were recorded at 37 °C over several hours. To simplify the ^{13}C−^{1}H HSQC spectra in the cysteine C_β−H region (δ = 25−32 for ^{13}C and $\delta \sim 3.2$ for ^{1}H) (*24*, *25*), a surface cysteine (Cys-41) was mutated to alanine, leaving only the two essential cysteines in the enzyme (Cys-83 and Cys-125). Cys-41 is remote from the active site, and the C41A mutant has essentially wild-type catalytic activity (Table 1). The protein was produced in the Zn^{2+}-substituted form, which has ~10% of the catalytic activity of the Fe^{2+} and Co^{2+} forms (*13*). The latter metals would cause paramagnetic line width broadening as well as perturb the chemical shift values.

At pH 9.5, C41A EcLuxS exhibited two sets of cysteine signals, a doublet at δ 30.2 (^{13}C)/3.10 (^{1}H) and δ 30.2/3.70 and an unresolved doublet at δ 30.6/3.25 (Figure 6A). As the pH decreased, the doublet at δ 30.6/3.25 gradually migrated to the δ 29.5/3.30 and 29.5/3.40 region. A plot of the ^{13}C chemical shift value against pH produced a sigmoidal curve, and data fitting revealed a single ionization event with a pK_a of 7.0 (Figure 6C). The other doublet (at δ 30.2/3.10 and 30.2/3.70), however, remained unchanged throughout the pH range that was tested (6.0−9.5) (Figure 6A,C). To assign the cysteine signals, a C41A/C83D double mutant was generated and analyzed under the same conditions. The double mutant exhibited a doublet at δ 30.4/3.30 at pH 8.0, which migrated to δ 29.5/3.30 and 29.5/3.40 as the pH decreased to 6.0 (Figure 6B), indicating that the pK_a of 7.0 belonged to Cys-125 and the unchanged doublet signals at δ 30.2/3.10 and 30.2/3.70 arose from Cys-83. A pK_a of 7.0 for Cys-125 provides a possible explanation for the instability of LuxS at acidic pH. Presumably, at pH <7, Cys-125 becomes protonated and therefore a less effective ligand for the metal ion, leading to protein denaturation. The lack of a pH-dependent change in Cys-83 signals over the pH range of 6.0−9.5 led us to conclude that the pK_a value of Cys-83 is <6. This interpretation is consistent with the results from our UV absorption studies and the fact that the ^{13}C chemical shift for Cys-83 (δ 30.2) is very similar to that of Cys-125 thiolate (δ 30.6).

DISCUSSION

pK_a and Function of Metal-Bound H_2O. Although Fe^{2+} is the native metal ion in LuxS, Co−LuxS has catalytic properties virtually identical to those of Fe−LuxS and is much more stable (*13*). In addition, the paramagnetic Co^{2+} exhibits characteristic spectra that are highly sensitive to coordination geometry and the nature of ligands, making it an excellent spectroscopic probe for the enzyme active-site environment (*26*). Our UV−vis studies of wild-type LuxS revealed a single ionization event with a pK_a of 10.4 (Figure 3A). We assigned this pK_a to the metal-bound water by the process of elimination, because mutation of none of the ionizable active-site residues [including Ser-6, His-11, Arg-39, Glu-57, Cys-84 (to Asp), and Tyr-89] resulted in loss of this ionization event. It should be noted that other ionization events might have occurred in the protein over the pH range of 7−12, but they did not cause detectable spectral changes of the Co^{2+} ion.

A pK_a of ~10 is very high for a water molecule bound to a tetrahedral Co^{2+} ion. As a comparison, the metal-bound water in E133A peptide deformylase, which has the same first-coordination sphere ligands as LuxS, has a pK_a of 6.0 (*27*). The substantially higher pK_a value in LuxS indicates that the outer-shell ligands in LuxS must influence the acidity of the metal-bound water. We hypothesize that the stabilization energy to maintain the H_2O molecule, or alternatively, the destabilization of the OH^- ion in the active site, largely benefits from the electrostatic repulsion from the active-site general acids/bases, i.e., Glu-57 and Cys-84. The negative charges on these residues should disfavor the formation of a third negative charge in the vicinity, thus destabilizing the metal−OH^- form and increasing the pK_a of metal-bound H_2O. The C84D mutation introduces a permanent negative charge into the active site (p$K_a \sim 4$ for aspartate), which mimics the electronic environment of the wild-type enzyme at physiological pH (pK_a < 6 for Cys-84). Indeed, the absorption spectra and the pH-dependent changes of C84D LuxS were similar to those of the wild-type enzyme. In C84A LuxS, elimination of the negative charge at position 84

removes the electrostatic repulsion that would otherwise destabilize the metal-bound OH^-, thus lowering the pK_a of metal-bound H_2O to <7. Therefore, the spectra of C84A LuxS correspond to the LuxS form with OH^- bound to the metal, and the appearance of two closely associated peaks at 600−700 nm in C84A does resemble the spectra of wild-type LuxS under basic pH conditions. For the same reason, C84S LuxS has a more normal pK_a value for its metal-bound water (<7) and exists in the metal-bound OH^- form at physiological pH. The observed spectral change of C84S LuxS at pH ≥11 (Figure 3D) can be articulated as follows. Serine typically has a pK_a of ∼16, but the same residue(s) that is responsible for reducing the pK_a of Cys-84 from ∼8.5 to <6 should also lower the pK_a of Ser-84. Therefore, the spectral change at pH >11 can be attributed to the ionization of Ser-84 to its alkoxide form. The observed effect of Cl^- ions on LuxS spectra can also be rationalized by the hypothesis given above. Wild-type and C84D LuxS exist in the metal-H_2O form at pH <10, and therefore, they are easily converted into the metal−Cl form by the addition of 2 M NaCl. C84A and C84S LuxS variants are more resistant to spectral perturbation by Cl^- ions because their metal-bound OH^- is more difficult to displace with the Cl^- ion.

Although complicated somewhat by active-site heterogeneity, the EPR data are also consistent with the interpretation given above. On the basis of the pH titrations monitored by UV−vis spectroscopy, the C84D mutant is believed to possess an aqua ligand (Co−H_2O) at pH 8. It possesses a nearly axial EPR spectrum that we interpret as a spectroscopic signature of a bound aqua ligand at the active-site Co^{2+}. Similar EPR spectra were observed for C84A LuxS under all pH conditions and the C84D mutant at pH 11. Although the origin of pH- and mutation-induced active-site heterogeneity is not understood at present, we take the similarity of spectral features here to indicate hydroxide coordination at the active-site Co^{2+}.

In summary, our spectroscopic data support the assignment of the pK_a of 10.4 to the metal-bound H_2O in wild-type and C84D LuxS. Thus, at physiological pH, the LuxS metal center exists in the metal-bound H_2O form. The relatively weak interaction between H_2O (relative to OH^-) and the metal ion makes it possible for the carbonyl oxygen of SRH to displace the bound water during catalysis. Indeed, Co−LuxS undergoes dramatic spectral changes during the catalytic cycle (*13*). Direct coordination to the metal ion by the C2 carbonyl oxygen of ketone intermediate **4** has previously been observed in cocrystal structural studies (*11*). Taken together, these data argue strongly for a Lewis acid function of the metal ion, as we had originally proposed (Figure 2).

Function of Active-Site Cysteine. Previous site-directed mutagenesis, kinetic analysis, and real-time ^{13}C NMR spectroscopic studies suggest that Cys-83 (in VhLuxS and EcLuxS, or Cys-84 in BsLuxS) functions as a GA/GB to catalyze the proton transfers at positions C1−C3 (*13*, *14*). The X-ray crystal structures of LuxS bound with two analogues of the enediolate intermediates revealed that the sulfur atom of Cys-84 is 3.4−4.1 Å from the C1−C3 positions of the ribose and properly oriented to serve as a GA/GB during catalysis (*12*). In this work, pH titration by $^{13}C-^{1}H$ HSQC NMR experiments showed no spectral change between pH 6.0 and 9.5, indicating that the pK_a of this cysteine must be <6 or >9.5. We assign the cysteine pK_a to <6 for several reasons. First, wild-type LuxS has spectral properties similar to those of the C84D mutant, which has a negative charge at position 84 and residual catalytic activity. Second, native LuxS (Fe^{2+} form) undergoes rapid inactivation under physiological conditions due to oxidation of Cys-84 into cysteic acid (*13*). A thiolate is more susceptible to oxidation. Finally, the pH profile of wild-type LuxS shows a single ionization event (ionization of Co−H_2O) over the pH range of 7.0−12 (Figure 3A). As vividly demonstrated by the difference between wild-type LuxS and the C84A mutant, a change in the charge state at position 84 should result in dramatic changes in the absorption spectra. The absence of such spectral change indicates that the pK_a of Cys-84 is either <7.0 or >12. A pK_a of >12 for a cysteine is highly unlikely. Thus, a pK_a of <6 makes Cys-84 an ideal GA/GB in the LuxS reaction; at the beginning of the catalytic cycle, Cys-84 is expected to be in the thiolate form, ready to abstract the C2 proton from SRH (Figure 2). The ionization state of Cys-125, which is one of the metal ligands, warrants some comments. Its pK_a of 7.0 is somewhat surprising, as we had expected it to be predominantly in the thiolate form at physiological pH, especially considering that a non-metal-coordinated thiolate group (Cys-83) is in its vicinity. However, a pK_a of ∼7 does provide a simple explanation for the observed instability of LuxS and peptide deformylase, which has an identical metal−ligand environment, at pH <7 (*27*).

Function of Arg-39. Arg-39 is an invariant active-site residue (*8*−*11*). However, it is rather distant from the metal ion and unlikely to directly affect the pK_a of the metal-bound H_2O, yet the R39M mutation decreased the catalytic activity by 1250-fold. We propose that Arg-39 exerts its effects by decreasing the pK_a value of Cys-84 (in BsLuxS) through electrostatic interaction between the positively charged arginine side chain and the thiolate ion. On the basis of this hypothesis, the R39M mutation would abolish the electrostatic interaction required to stabilize the thiolate ion and therefore return the pK_a of Cys-84 to its normal value. A protonated Cys-84 (at neutral pH) would in turn remove the electrostatic repulsion between the thiolate ion and a metal-bound OH^-, resulting in a lower pK_a for the metal-bound water. This is indeed the case for R39M LuxS, whose absorption spectra do not exhibit ionization at pH >10. Instead, it undergoes two ionization events with pK_a values of ∼6.4 and 8.6 (Figure 3E). We tentatively assign the pK_a values to Cys-84 and the metal-bound water, although we do not know which pK_a is associated with Cys-84. As expected, introduction of the R39M mutation into the C84D or C84A mutant has a much weaker effect on their properties. For example, the R39M/C83D double mutant has essentially the same catalytic activity toward SRH and ketone **4** as the C83D mutant (Table 1). R39M/C84D BsLuxS shows a single ionization event, although the pK_a value (9.9) is slightly lower than that of the wild-type enzyme (10.4). Presumably, due to its lower pK_a, Asp-84 can exist in the ionized state regardless of the ionization status of Arg-39. Likewise, C84A and R39M/C84A mutants had similar absorption spectra and pH dependence (or independence). R39M mutation further reduced the activity of C83S LuxS by ∼7-fold (Table 1). This can be rationalized in a way that Arg-39 is needed to

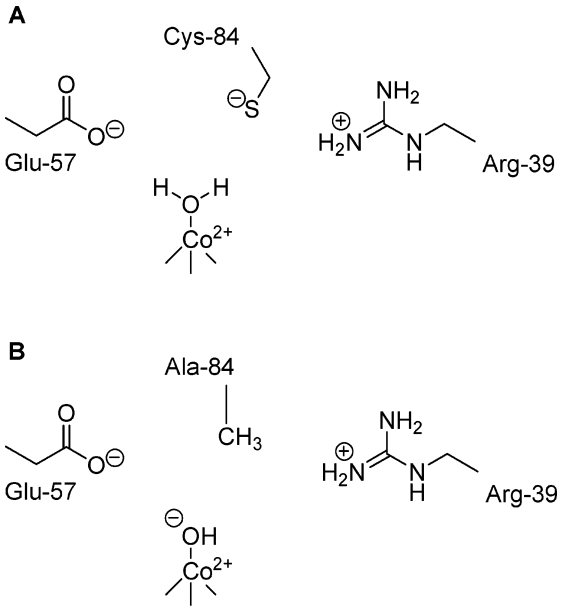

FIGURE 7: Ionization state of BsLuxS active-site residues: (A) wild-type LuxS and (B) C84A LuxS.

stabilize the alkoxide side chain of Ser-83 as discussed previously.

Implication for the LuxS Catalytic Mechanism. On the basis of the results from this and earlier work, we propose that the ionization state of active-site residues in the active form of LuxS is as shown in Figure 7A. Arg-39 is positively charged, and it reduces the pK_a of Cys-84 to <6 through electrostatic interactions. The negative charges on Cys-84 thiolate and Glu-57 carboxylate destabilize a metal-bound hydroxide form through electrostatic repulsion. As a result, the fourth ligand of the catalytic metal ion is a water molecule at physiological pH, which can be displaced by the carbonyl oxygen of SRH during catalysis. Mutation of Cys-84 to an alanine eliminates the electrostatic repulsion, and a hydroxide ion is bound to the metal ion (Figure 7B). The results provide additional support for the proposed catalytic mechanism of LuxS (Figure 2).

ACKNOWLEDGMENT

We thank Dr. Chunhua Yuan for assistance with the $^{13}C-^{1}H$ HSQC experiments.

REFERENCES

1. Federle, M. J., and Bassler, B. L. (2003) Interspecies communication in bacteria, *J. Clin. Invest. 112*, 1291−1299.
2. Xavier, K. B., and Bassler, B. L. (2003) LuxS quorum sensing: More than just a numbers game, *Curr. Opin. Microbiol. 6*, 191−197.
3. Miller, C. H., and Duerre, J. A. (1968) *S*-Ribosylhomocysteine cleavage enzyme from *Escherichia coli*, *J. Biol. Chem. 243*, 92−97.
4. Surette, M. G., Miller, M. B., and Bassler, B. L. (1999) Quorum sensing in *Escherichia coli*, *Salmonella typhimurium*, and *Vibrio harveyi*: A new family of genes responsible for autoinducer production, *Proc. Natl. Acad. Sci. U.S.A. 96*, 1639−1644.
5. Schauder, S., Shokat, K., Surette, M. G., and Bassler, B. L. (2001) The LuxS family of bacterial autoinducers: Biosynthesis of a novel quorum-sensing signal molecule, *Mol. Microbiol. 41*, 463−476.
6. Miller, S. T., Xavier, K. B., Campagna, S. R., Taga, M. E., Semmelhack, M. F., Bassler, B. L., and Hughson, F. M. (2004) *Salmonella typhimurium* recognizes a chemically distinct form of the bacterial quorum-sensing signal AI-2, *Mol. Cell 15*, 677−687.
7. Chen, X., Schauder, S., Potier, N., van Dorsselaer, A., Pelczer, I., Bassler, B. L., et al. (2002) Structural identification of a bacterial quorum-sensing signal containing boron, *Nature 415*, 545−549.
8. Lewis, H. A., Furlong, E. B., Laubert, B., Eroshkina, G. A., Batiyenko, Y., Adams, J., et al. (2001) A structural genomics approach to the study of quorum sensing: Crystal structures of three LuxS orthologs, *Structure 9*, 527−537.
9. Hilgers, M. T., and Ludwig, M. L. (2001) Crystal structure of the quorum-sensing protein LuxS reveals a catalytic metal site, *Proc. Natl. Acad. Sci. U.S.A. 98*, 11169−11174.
10. Ruzheinikov, S. N., Das, S. K., Sedelnikova, S. E., Hartley, A., Foster, S. J., Horsburgh, M. J., et al. (2001) The 1.2 Å structure of a novel quorum-sensing protein, *Bacillus subtilis* LuxS, *J. Mol. Biol. 313*, 111−122.
11. Rajan, R., Zhu, J., Hu, X., Pei, D., and Bell, C. E. (2005) Crystal structure of *S*-ribosylhomocysteinase (LuxS) in complex with a catalytic 2-ketone intermediate, *Biochemistry 44*, 3745−3753.
12. Shen, G., Rajan, R., Zhu, J., Bell, C. E., and Pei, D. (2006) Design and synthesis of substrate and intermediate analogue inhibitors of *S*-ribosylhomocysteinase, *J. Med. Chem. 49*, 3003−3011.
13. Zhu, J., Dizin, E., Hu, X., Wavreille, A., Park, J., and Pei, D. (2003) *S*-Ribosylhomocysteinase (LuxS) is a mononuclear iron protein, *Biochemistry 42*, 4717−4726.
14. Zhu, J., Hu, X., Dizin, E., and Pei, D. (2003) Catalytic mechanism of *S*-ribosylhomocysteinase (LuxS): Direct observation of ketone intermediates by ^{13}C NMR spectroscopy, *J. Am. Chem. Soc. 125*, 13379−13381.
15. Zhu, J., Patel, R., and Pei, D. (2004) Catalytic mechanism of *S*-ribosylhomocysteinase (LuxS): Stereochemical course and kinetic isotope effect of proton-transfer reactions, *Biochemistry 43*, 10166−10172.
16. Zhu, J., Dhimitruka, I., and Pei, D. (2004) 5-(2-Aminoethyl)dithio-2-nitrobenzoate as a more base-stable alternative to Ellman's reagent, *Org. Lett. 6*, 3809−3812.
17. Ellman, G. L. (1959) Tissue sulfhydryl groups, *Arch. Biochem. Biophys. 82*, 70−77.
18. O'neal, J. S., and Schulman, S. G. (1984) Simplification of the Robinson-Biggs spectrophotometric treatment of overlapping prototropic equilibria by use of isosbestic points, *Anal. Chim. Acta 164*, 263−266.
19. Crane, E. J., III, Vervoort, J., and Claiborne, A. (1997) ^{13}C NMR analysis of the cysteine-sulfenic acid redox center of enterococcal NADH peroxidase, *Biochemistry 36*, 8611−8618.
20. Bradford, M. M. (1976) A rapid and sensitive method for the quantitation of microgram quantities of protein utilizing the principle of protein-dye binding, *Anal. Biochem. 72*, 248−254.
21. Bertini, I. (1983) *Coordination Chemistry of Metalloenzymes*, *I* (Bertini, I., et al., Eds.) pp 1−18, D. Reidel Publishing Co., Dordrecht, The Netherlands.
22. Bennett, B. (2002) EPR of Co(II) as a structural and mechanistic probe of metalloprotein active sites: A review of studies on aminopeptidase, *Curr. Top. Biophys. 26*, 49−57.
23. Bennett, B., and Holz, R. C. (1997) EPR studies on the mono- and dicobalt(II) substituted forms of the aminopeptidase from *Aeromonas proteolytica*. Insight into the catalytic mechanism of dinuclear hydrolases, *J. Am. Chem. Soc. 119*, 1923−1933.
24. Sharma, D., and Rajarathnam, K. (2000) ^{13}C NMR chemical shifts can predict disulfide bond formation, *J. Biomol. NMR 18*, 165−171.
25. Statistics from the BioMagResBank database (http://www.bmrb.wisc.edu).
26. Maret, W., and Vallee, B. L. (1993) Cobalt as probe and label of proteins, *Methods Enzymol. 226*, 52−71.
27. Rajagopalan, P. T. R., Grimme, S., and Pei, D. (2000) Characterization of cobalt(II)-substituted peptide deformylase: Function of the metal ion and the catalytic residue Glu-133, *Biochemistry 39*, 779−790.

BI061434V